# Clear Memory-Augmented Auto-Encoder for Surface Defect Detection

Wei Luo<sup>a,\*</sup>, Tongzhi Niu<sup>a,\*</sup>, Lixin Tang<sup>a,†</sup>, Wenyong Yu<sup>a</sup>, Bin Li<sup>a</sup>

<sup>a</sup> School of Mechanical Science and Engineering, Huazhong University of Science and Technology, Wuhan 430074, China

\* Wei Luo and Tongzhi Niu contributed equally to this work

<sup>†</sup>Lixin Tang is the corresponding author, E-mail address: lixintang@hust.edu.cn

#### Abstract:

In surface defect detection, due to the extreme imbalance in the number of positive and negative samples, positive-samples-based anomaly detection methods have received more and more attention. Specifically, reconstruction-based methods are the most popular. However, exiting methods are either difficult to repair abnormal foregrounds or reconstruct clear backgrounds. Therefore, we propose a clear memory-augmented auto-encoder. At first, we propose a novel clear memory-augmented module, which combines the encoding and memory-encoding in a way of forgetting and inputting, thereby repairing abnormal foregrounds and preservation clear backgrounds. Secondly, a general artificial anomaly generation algorithm is proposed to simulate anomalies that are as realistic and feature-rich as possible. At last, we propose a novel multi scale feature residual detection method for defect segmentation, which makes the defect location more accurate. CMA-AE conducts comparative experiments using 11 state-of-the-art methods on five benchmark datasets, showing an average 18.6% average improvement in F1-measure.

**Keywords**: Surface defect detection; Anomaly detection; Clear memory-augmented; Artificial anomaly images; Multi scale feature residual.

## 1. Introduction

In the industrial, due to the complex of manufacturing process, surface defects are common in some industrial products such as fabric [1] and steel [2]. These defects not only lead to poor user experience, but also may cause industrial accidents. For an example, surface defects of steel may reduce Contact Fatigue Strength of the material. Therefore, defects inspection is an important method to achieve quality management.

Over the past decades, various surface defect detection methods have been proposed. These methods can be broadly divided into two categories, including traditional methods and deep-learning based methods. Traditional methods mainly extract features manually and set thresholds to detect defects. Aiger and Talbot [3] proposed Phase-Only Transform (PHOT) to detect the irregular defects in background. Xie and Mirmehdi [4] presented a Gaussian mixed model to detect and localize defects. Low-pass filtering with curvature analysis (LCA) was proposed by Tsai and Huang [5] to remove periodic textural patterns. However, the feature extraction ability of the above methods is limited and the robustness is poor. As a data-driven method, deep learning can automatically extract features by training a large amount of data, with strong feature extraction ability and good generalization.

Most deep learning based methods are supervised learning approaches. PGA-Net [6] proposed a pyramid feature fusion and global context attention network for pixel-wise detection. Tabernik et al. [7] presented a segmentation-based deep learning architecture for surface defect detection. However, the above methods require a large number of defective samples and corresponding labels, which is difficult to obtain in the industrial field. Firstly, the number of defect-free samples is much larger than that of defective samples, and unknown defect types may occur in the process of production. Therefore, data collection becomes the biggest challenge in defect detection tasks. Secondly, sample labelling requires experienced engineers to spend a lot of time and effort, which is time-consuming and high-labor cost. These factors above limit the application of supervised learning in the industrial fields. In contrast, unsupervised learning methods show great potential as it only requires unlabeled normal samples for training. In recent years, unsupervised anomaly

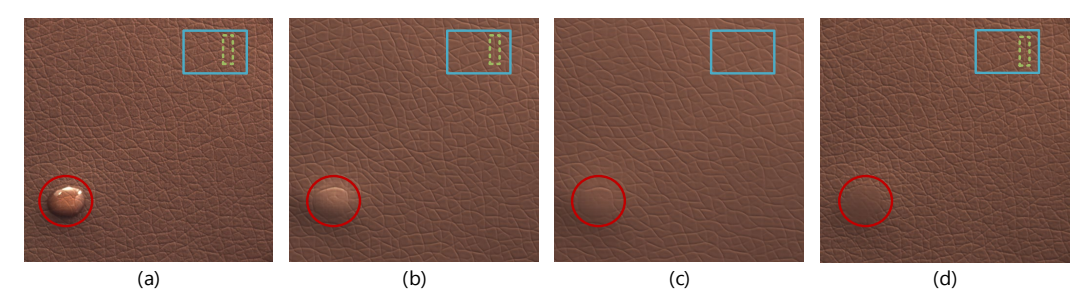


Fig. 1. Reconstruction results of different methods. (a) is the original image, (b) is reconstructed using AE [15], (c) is reconstructed using MemAE [16] and (d) is reconstructed using CMA-AE

detection has received increasing attention. Many anomaly detection methods are applied to defect detection and made great progress. RIAD [8] treat anomaly detection as a reconstruction-by-inpainting problem and achieved excellent results in image anomaly detection. Zhang et al. [9] proposed a deep adversarial anomaly detection method with task-specific features for anomaly detection. Cho et al. [10] proposed a normal features distribution model in an unsupervised manner for video anomaly detection. Ribeiro et al. [11] proposed a convolutional auto-encoder architecture to learn normal behavior and use the model for anomaly detection. Zhou et al. [12] proposed a patch-level autoencoder combined with a context-enhanced autoregressive network for anomaly detection. Chen et al. [13] proposed an end-to-end pipeline named NM-GAN, which assembles an encoder-decoder reconstruction network and a CNN-based discriminative network. Yang et al. [14] mainly proposed deep features corresponding to anomaly detection and segmentation.

For anomaly detection, trained on the normal samples, the model is expected to produce larger reconstruction/generate errors for the anomalies than that for the normal ones. Therefore, the two most important capabilities of the model are the ability to reconstruct normal backgrounds and the ability to repair abnormal foregrounds. Because of the under-designed representation of the latent space, common AE [15] have the capability of the former, but not the latter. MemAE [16] proposed an improved AE that repairs the abnormal foregrounds by editing latent codes with a memory-

augment module. The proposal of MemAE greatly enhances the repair ability of abnormal foreground, but at the same time weakens the ability to reconstruct normal background, as shown in Fig. 1. Specifically, MemAE uses the encoding from the encoder as a query to retrieve the most relevant memory items for decoding, which completely replaces the input features, resulting in loss of detail. Therefore, we propose a novel clear memory-augmented module (CMAM), which combines the encoding and memory-encoding in a way of inputting and forgetting, thereby repairing abnormal foregrounds and preservation clear backgrounds.

There are two improvements in the CMAM. At first, inspired by LSTM [17], the way of inputting and forgetting is designed to improve the memory mechanism. We try to erase anomalous foregrounds in coding through a forget gate, and then use the memory-encoded information to inpainting the erased features through an input gate, resulting in a clear reconstruction map. Secondly, to learn how to forget and input, we proposed a two-stage training strategy. At the first stage, training with normal samples, the memory content is updated together with the encoder and decoder. At the second stage, the memory content is no longer updated, and the input and forgetting abilities are learned by repairing artificial anomalies in the samples.

Recently, artificial anomalies have been widely used to enhance the models. AFEAN [18] generated artificial anomalies by combining the defect-free images and random masks. Lv et al. [19] proposed to use redundant features in natural images to simulate defects. Cutpaste [20] cut a small rectangular area from a normal training image and paste it back to an image at a random location. But as all as we know, existing artificial anomalies are designed based on human experience and can only simulate limited real anomalies. Therefore, we propose a general artificial anomaly generation algorithm (GAAGA) to simulate anomalies that are as realistic and feature-rich as

possible. We first assume that the features of natural images are redundant enough to simulate almost all anomalous features. And the blur of normal backgrounds can be regarded as degenerate anomalies. Inspired by Cutpaste, natural images and the blurring images of normal backgrounds as image patches are both paste at a random location of a large image.

Finally, in anomaly detection, the pixel gap between the original image and the reconstructed image is still used for defect segmentation in anomaly detection, which will cause a lot of noise and lead to the occurrence of false detection, As show in Fig. 8, 9. As we can see, individual pixel has no semantics, normal and abnormal are context-dependent semantic descriptions. Whether it is filters of traditional methods or convolutional neural networks, contextual relevance is considered to be the key to image processing. Therefore, replacing pixel gaps with feature gaps is a more feasible approach. Since the size of the anomaly is ambiguous, we proposed a novel multi scale feature residual (MSFR) detection method for defect segmentation.

There are two advantages in MSFR. Firstly, the residual between original feature map and reconstructed feature map guarantees the correlation between pixels, since an element in the feature map corresponds to pixels in one region of the original image. Secondly, different feature maps have different receptive fields, multiple feature map residuals are used to obtain multi-scale information.

To sum up, the main contributions of our work are as follows:

- a) We propose a novel clear memory-argument module (CMAM), which solves the problem of poor normal background reconstruction in MemAE [16]. A two-stage training strategy is adopt to improve the ability to reconstruct normal background and the ability to repair abnormal foreground respectively.
- b) We propose a novel multi scale feature residual method for defect segmentation (MSFR),

which effectively solves the noise problem caused by using the pixel gap between the original image and the reconstructed image for defect segmentation, and makes the defect location more accurate.

c) We also propose a novel artificial anomaly generation algorithm to simulate various possible real defects in industry.

The rest of this article is organized as follows. The section II introduces the related works of anomaly detection. In section III, the proposed CMA-AE and MSFR are elaborated and discussed in detail. Section IV designs extensive experiments to demonstrate the performance of CMA-AE and MSFR. Finally, section V summarize the paper.

## 2. Related works

In recent years, the success of deep learning model training is generally determined by the number of representative training samples and the quality of the annotation. Therefore, anomaly detection based on positive samples without labels have received more and more attention. Many reconstruction-based anomaly detection methods have been proposed, most of which can be classified into two categories, including Auto-Encoder (AE) [15], Generate Adversarial Nets (GANs) [21] and their variants.

AE-based models can learn encoded features in the latent feature domain by training normal samples, and then reconstruct the background images from them. During testing, the output of anomaly samples is expected to be unknown, with a large gap with the samples. In order to enhance the representation ability, many methods have paid a lot of efforts in the design of network structure and loss function. Mei et al. [22] proposed MSCDAE, which uses a Gaussian pyramid structure to

obtain different receptive fields to generate more realistic background images. Yang et al. [23] proposed a fully convolutional AE based on multi-scale feature clustering to reconstruct image backgrounds. These AE-based models train the model by minimizing the mean absolute error (L1) or squared Euclidean error (L2) between the original image and the reconstructed image, ignoring the structural information of the image, which easily leaded to blurred reconstructed images. Therefore, Bergmann et al. [24] proposed AE-SSIM, which applies structural similarity to an autoencoder for image background to inspect defects. However, due to the strong generalization ability of the neural networks, some defects will also be perfectly reconstructed. And none of the above methods have the ability to deal with abnormal features properly. To solve this problem, MemAE[16] proposed a memory-augmented autoencoder to improve the performance of the autoencoder by obtaining reconstruction from selected memory contents records of the normal data. MemAE can repair the abnormal samples well, amplify abnormal reconstruction errors, which strength the reconstruction error as the anomaly detection criterion. Recently, many improved methods based on memory mechanisms have been proposed. TrustMAE [25] presented a noise-resilient and unsupervised framework for product defect detection. Hou et al. [26] explain image reconstruction from the perspective of feature map division and assembly, and thus proposed a block-wise memory module. However, from the experimental results, MemAE repairs the abnormal foreground well and blurs the normal background at the same time.

Recently, GANs [21] have played an important role in the field of style transfer [27] and image generation [28], which shows that GANs have strong generative ability. Schlegl et al. [29] firstly applied GANS in the field of anomaly detection. Since the original GAN lacks the mapping from the image domain to the latent feature domain, f-AnoGAN [30], AAE [31], OCGAN [32], and

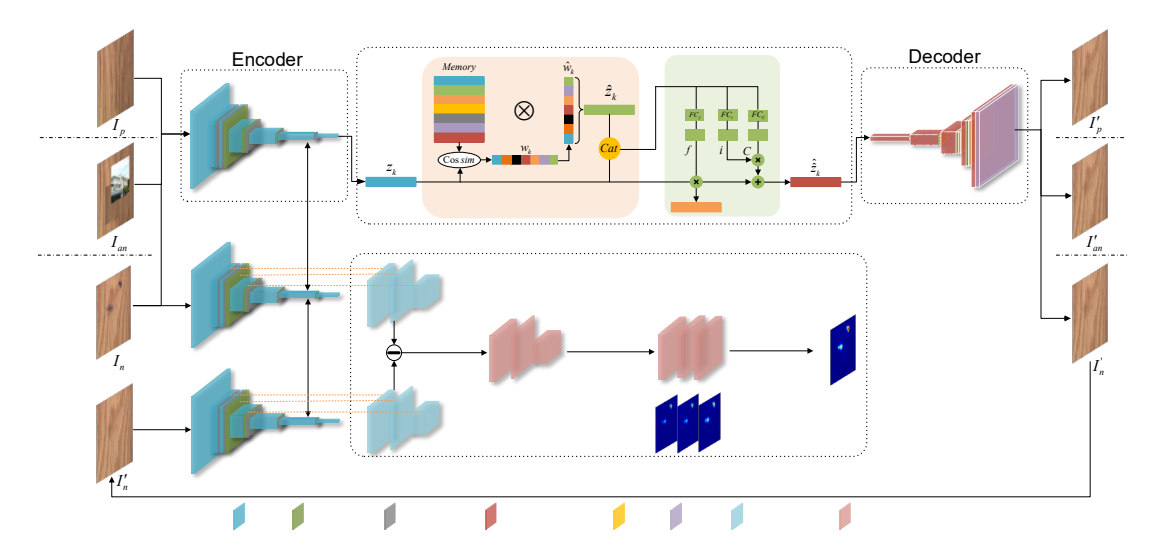


Fig. 2. Overall architecture of the proposed CMA-AE in the train and test stages. CMA-AE consists of a CMAM, a MSFR, an encoder and a decoder. During training, positive samples and artificial negative samples are propagated forward in two stages. During testing, the abnormal area of negative samples is obtained by MSFR.

GPND [33] are proposed. Since then, many potential anomaly detection models base on GAN have been proposed. Ganomaly [34] proposed an encoder-decoder-encoder framework to minimize the distance between original and the reconstructed image in both image space and latent feature space. In order to increase the details of the reconstructed image, Skip-Ganomaly [35] combines Skip-connection and Ganomaly to reconstruct a more realistic image background. However, due to the introduction of the encoder-decoder networks structure, the above GANs-based methods are also unable to properly handle abnormal features. Therefore, Yang et al. [18] proposed AFEAN to eliminate the effect of defect reconstruction by editing defect sample features. Niu et al. [36] proposed a memory-augmented adversarial autoencoder for defect detection, which edit the latent features through memory mechanism and ConvLSTM [37]. In general, most of these methods are trained only on positive samples, and localize defects through residuals between original and reconstructed images. However, these methods do not achieve good performance because they exploit the pixel gap between the original image and the reconstructed image to locate defects, resulting in inaccurate defect localization and a large amount of noise.

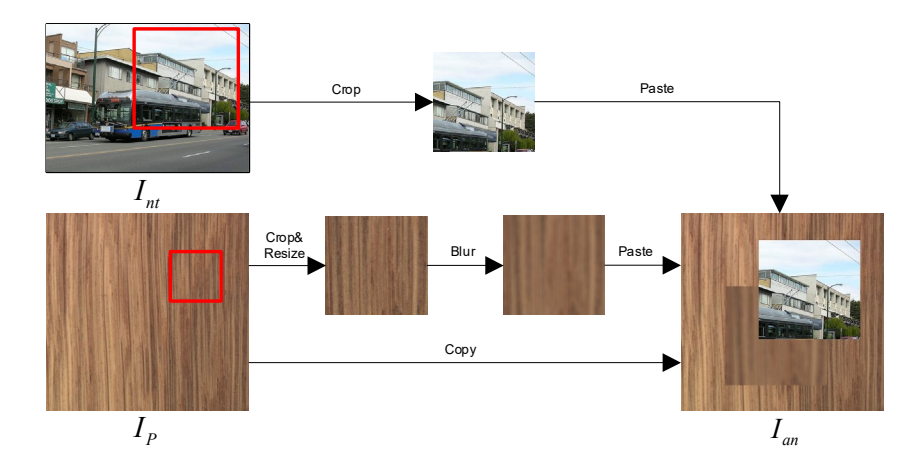


Fig. 3. General artificial anomaly generation algorithm. The artificial negative samples are obtained by Crop-and-Paste of natural images and positive samples.

# 3. Methodology

In this section, the proposed Clear Memory-Augmented Auto-Encoder (CMA-AE) is introduced in detail. Firstly, the overall network architecture is briefly introduced. Then, the main modules of CMA-AE are divided into five parts for detailed introduction, including the clear memory-augmented module (CMAM), general artificial anomaly generation algorithm (GAAGA), the multi scale feature residual (MSFR), the Encoder and the Decoder and the two-stage training strategy. Finally, the details of the reconstruction loss and the design of the loss function are discussed.

## 3.1 Overall network architecture of CMA-AE

The overall structure of the CMA-AE is shown in Fig 2. The proposed CMA-AE consists of five major components-AAGA (for generating artificial anomaly images), Encoder (for extracting latent features from images), CMAM (for inpainting anomalous foregrounds and reconstructing normal backgrounds in latent space), Decoder (for reconstructing images from latent features) and Multi Scale Feature Residual (for anomaly segmentation).

The training phase is divided into two stages. At the first stage, our training set contains only positive samples  $I_p$ . Firstly, we divide the images into  $k^{th}$  patches and extract the latent features  $z_k$  by Encoder. Secondly, the latent features  $z_k$  are re-encoded by CMAM to get memorized latent features  $\hat{z}_k$ . Finally, the  $\hat{z}_k$  is fed into Decoder to get reconstruct images  $I'_p$ . The CMAM, Encoder, and Decoder are optimized simultaneously. At the second stage, the Memory of CMAM is no longer optimize. To make the model better address abnormal features, artificial negative samples  $I_{am}$  are generated by GAAGA and used as training set. Through the forgetting and inputting mechanism of CMAM, the abnormal foreground is repaired, the normal background is reconstructed, and finally the images  $I'_{am}$  is obtained.

During testing phase, the negative samples  $I_n$  are reconstructed by Encoder, CMAM, and Decoder to obtain the images  $I'_n$ . MSFR uses multi-scale information of input  $I_n$  and output  $I'_n$  for more accurate anomaly segmentation.

# 3.2 General artificial anomaly generation algorithm

Due to the limitations of artificial design, artificial anomaly samples usually can only simulate a few real anomalies. Inspired by Cutpaste [20], we proposed a GAAGA that cuts an image patch and pastes at a random location of an image, as shown in Fig. 3. First, based on the feature redundancy of natural images relative to industrial images, we randomly crop a 256×256 patch from a natural image in the ImageNet dataset [38]. Then, to more closely simulate anomalous features, we also randomly crop the patch from normal samples and resize them to 256×256 before blurring. In particular, blurring allows patches to be considered degenerate anomalies, and resizing enables the networks to learn not the ability to deblur, but the ability to repair anomalies. Finally, the patches obtained in steps 1 and 2 are randomly paste into the normal samples, as follows:

Table I CMA-AE Architecture

Operation	Kernel	Strides	Padding	Features Maps/Unit	s BN?	Activation function		
Encoder						Input: x=[B,3,64,64]		
Conv	4x4	2x2	1	3,32				
Conv	3x3	1x1	1	32,32	$\checkmark$	LeakyReLU		
Conv	4x4	2x2	1	32,64	$\checkmark$	LeakyReLU		
Conv	4x4	2x2	1	64,128	$\checkmark$	LeakyReLU		
Conv	4x4	2x2	1	128,256	$\checkmark$	LeakyReLU		
Conv	4x4	1x1	0	256,512				
CMAM					I	nput: x=[B,512,1,1]		
FC				1024,512		Softmax		
FC				1024,512		Softmax		
FC				1024,512		Tanh		
Decoder						Input: x=[B,512,1,1]		
T.Conv	4x4	1x1	0	512,256				
T.Conv	4x4	2x2	1	256,128	$\checkmark$	ReLU		
T.Conv	4x4	2x2	1	128,64	$\checkmark$	ReLU		
T.Conv	4x4	2x2	1	64,32	$\checkmark$	ReLU		
T.Conv	3x3	1x1	1	32,32	$\checkmark$	ReLU		
T.Conv	4x4	2x2	1	32,3		Tanh		
Others:								
	Batch:				Size(B) 512			
	Optimizer:			A	$Adam(\alpha=0.0002,\beta=0.5)$			
	LeaklyReLU:				Slope 0.2			

$$I_{an} = paste(I_p, crop(I_{nt}), blur(resize(crop(I_p)))))$$
 (1)

where the positive samples and natural samples are represented by  $I_p$ ,  $I_{nl}$ . The operations of randomly crop, resize and blur are represented by crop(), resize(), and blur().  $paste(x_1,x_2,x_3)$  represents the operation of randomly pasting  $x_2$ ,  $x_3$  onto  $x_1$ .

## 3.3 Encoder and Decoder

In the reconstruction task, the images are mapped to the feature space by the encoder, and then mapped to the image space by the decoder. By setting an information bottleneck, a dimensionality-reduced data representation is obtained in the feature space. Considering the representation ability and computational cost, we design symmetric encoders and decoders, as depicted in Table I.

In the encoder,  $4\times4$  convolution kernels with a  $2\times2$  strides are used for dimensionality reduction. In order to obtain a larger receptive field, the second layer of the encoder adopts  $3\times3$  convolution kernels with strides of  $1\times1$ . Symmetric, the decoder uses  $4\times4$  deconvolution kernels with a  $2\times2$  strides and the penultimate layer uses  $3\times3$  deconvolution kernels with strides of  $1\times1$ .

# 3.4 Clear memory-augmented module

In order to make the network capable of repairing abnormal foreground and reconstructing normal background at the same time, based on MemAE [16], we propose a CMAM. As shown in Fig. 4, the CMAM includes memory-augmented module (MAM) and feature repair module (FRM). With MAM, we can get de-anomaly coding  $\hat{z}_k$  but lose details. But at the same time, the coding  $z_k$  obtained by encoder is rich in details. Therefore, FRM is proposed, which uses forget gates to erasure anomalous foregrounds in coding to get  $\hat{z}_k'$ . And then we use the memory-encoded information to repair the erased features through input gates to obtain  $\hat{z}_k$ . Furthermore, to elucidate the effectiveness of the proposed method, we feed the encoding obtained at each step into the decoder to obtain the corresponding image.

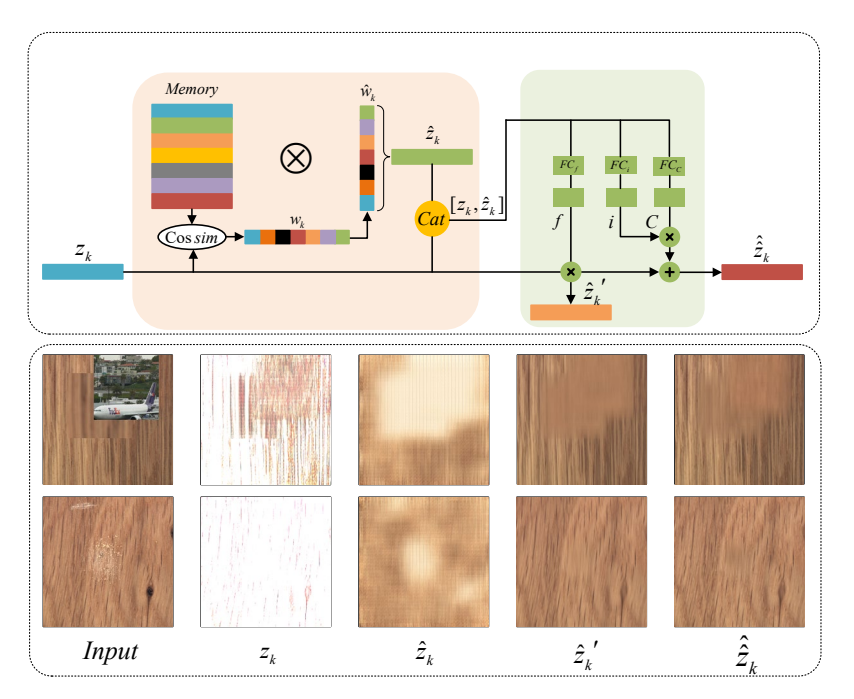


Fig. 4. Diagram of proposed clear memory-augmented module (CMAM). The CMAM includes memory-augmented module (MAM) and feature repair module (FRM). And we show the image obtained by the decoder at each stage of encoding.

#### 3.4.1 Memory-Argument Module

In MAM, the encoding from the encoder is used as a query to retrieve the most relevant memory items from the memory bank for decoding to get de-anomaly coding, as shown in Fig. 4.

The memory bank is used to record the prototypical normal patterns during training, implemented as a matrix  $M \in \mathbb{R}^{N \times C}$ , where N represents the number of memory items, and C represents the fixed dimension. Specifically, we set C equal to the dimension of the latent feature vector  $z_k \in \mathbb{R}^{1 \times C}$ , which denotes features of the  $k^{th}$  patch in the input image. And  $m^i \in \mathbb{R}^{i \times C} (i \in \{1, 2, ..., N\})$  is used to refer to the  $i^{th}$  memory item of M. We define the memory bank as a content addressable memory [39,40] with a specific addressing scheme.

The memory-coding  $\hat{z}_k$  is addressed by the attention weight vector  $w_k \in R^{N \times 1}$ .  $w_k^i (i \in \{1,2,...,N\}) \text{ is obtained by computing the cosine similarity between the input latent}$  feature vector  $z_k$  and each item  $m^i$  in the memory bank, as follows:

$$w_{k}^{i} = \frac{\exp(\frac{z_{k}(m^{i})^{T}}{\|z_{k}\| \|m^{i}\|})}{\sum_{j=1}^{N} \exp(\frac{z_{k}(m^{j})^{T}}{\|z_{k}\| \|m^{j}\|})}$$
(2)

Where  $\|\cdot\|$  denotes the modulus length of the vector. Additionally, items with attention weights less than 1/N are removed and renormalized, as follows:

$$\hat{w}_k^i = \frac{\max(w_k^i - \frac{1}{N}, 0) \cdot w_k^i}{|w_k^i - \frac{1}{N}| + \varepsilon}$$
(3)

Where  $\max(\cdot,0)$  is ReLU activation, and  $\mathcal{E}$  is a very small positive scalar. After the shrinkage, we renormalized  $\hat{w}_k$  by letting  $\hat{w}_k^i = \hat{w}_k^i / \|\hat{w}_k\|$ . Then  $\hat{z}_k$  is computed as follows:

$$\hat{z}_{k} = \hat{w}_{k} M = \sum_{i=1}^{N} \hat{w}_{k}^{i} m^{i} . \tag{4}$$

To further improve the sparsity of the attention weight vector  $\hat{w}$  during training, sparse loss function is proposed:

$$L_{s} = \sum_{k=1}^{K} \sum_{i=1}^{N} -\hat{w}_{k}^{i} \cdot \log(\hat{w}_{k}^{i}).$$
 (5)

The shrinkage operation in (3) and this sparse loss function in (5) jointly improve the sparsity of the attention weights.

### 3.4.2 Feature repair module

The  $z_k$  obtained by the Encoder and the de-anomaly  $\hat{z}_k$  getting with MAM are complementary in features. Therefore, we concatenate  $z_k$  and  $\hat{z}_k$  to get  $[z_k, \hat{z}_k]$ . The model is represented in (6)-(10). At first, the forget gate erasure anomalous foregrounds in the coding with a certain probability [as shown in (6)]. Then, the features of normal background are obtained by input gate [as shown in (7) and (8)]. Finally, the erased features are repaired to a normal background with clear details [as shown in (9) and (10)].

## a) Forget Gate:

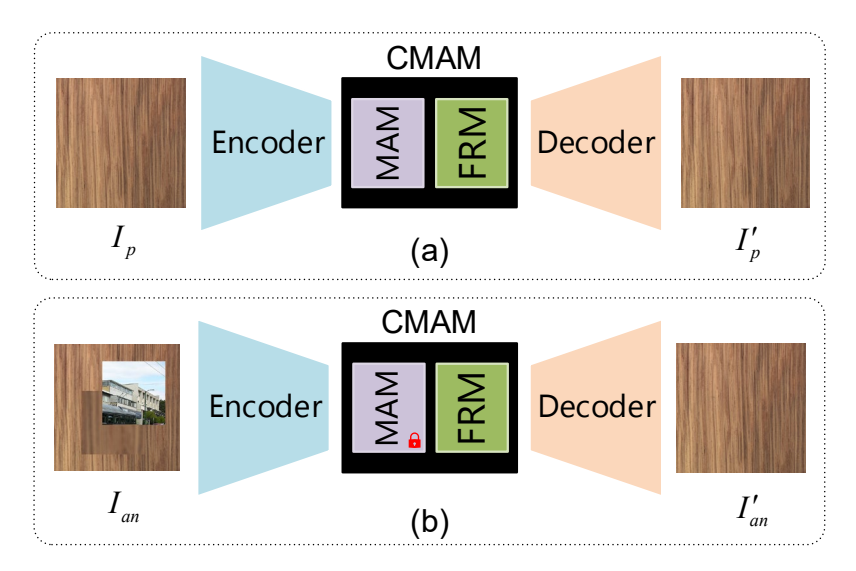


Fig 5. Illustration of the tow-stage training of CMA-AE. (a) Training stage 1, trained with positive samples, the Encoder, Decoder, MAM are updated together. (b) Training stage 2, trained with artificial negative samples, CMAM is no longer update.

$$f = \sigma(W_f \cdot [z_k, \hat{z}_k] + b_f) \tag{6}$$

b) Input Gate:

$$i = \sigma(W_i \cdot [z_k, z] + b_c) \tag{7}$$

$$C = \tanh(W_c \cdot [z_k, z] + b_c) \tag{8}$$

c) Forget-and-input update:

$$\hat{z}_k = f \cdot \hat{z}_k \tag{9}$$

$$\hat{\hat{z}}_k = \hat{z}_k + i \cdot C \tag{10}$$

where f, i, C are 2-D tensors,  $\sigma(\cdot)$  is softmax function,  $\tanh(\cdot)$  is the tanh function. And  $W_f$ ,  $W_i$  and  $W_c$  are the weights of fully connection layers,  $b_f$ ,  $b_i$ ,  $b_f$  are the biases of fully connection layers.

#### 3.4.3 Two-stage training strategy

As mentioned above, it is difficult to make the model have the ability to reconstruct normal background and repair abnormal foreground at the same time in one stage of training. Therefore, we proposed a two-stage training strategy, as shown in Fig. 5. In the first procedure, the model is optimized by training positive samples so that the CMAM record prototypical patterns of normal

#### Algorithm 1: Two-stage training strategy

Data: A generated dataset composed of positive images and artificial negative images

Input: Encoder, Decoder, CMAM (MAM, FRM)

Parameters: Iterations  $T_1$  and  $T_2$ , learning rate  $\alpha$ 

Training phase 1:

for  $i = 1, 2, ..., T_1$  do

- 1. Extract patches from normal images
- 2. Calculate partial derivatives:

$$\nabla_{\textit{Encoder}} L_{l}$$
,  $\nabla_{\textit{CMAM}} L_{l}$ ,  $\nabla_{\textit{Decoder}} L_{l}$ 

3. Superpose partial derivatives and renew models

$$Encoder \leftarrow Encoder + \alpha \times \nabla_{Encoder} L_1$$

$$CMAM \leftarrow CMAM + a \times \nabla_{CMAM} L_1$$

$$Decoder \leftarrow Decoder + \alpha \times \nabla_{Decoder} L_1$$

end

for  $i = 1, 2, ..., T_2$  do

- 1. fixed the weights of MAM
- 2. Extract patches from artificial anomaly images
- 3. Calculate partial derivatives:

$$\nabla_{{\scriptscriptstyle Encoder}} L_{\scriptscriptstyle 2} \;,\;\; \nabla_{{\scriptscriptstyle FRM}} L_{\scriptscriptstyle 2} \;,\;\; \nabla_{{\scriptscriptstyle Decoder}} L_{\scriptscriptstyle 2}$$

4. Superpose partial derivatives and renew models

$$\begin{aligned} FRM \leftarrow FRM + \alpha \times \nabla_{FRM} L_2 \\ Encoder \leftarrow Encoder + \alpha \times \nabla_{Encoder} L_2 \\ Decoder \leftarrow Decoder + \alpha \times \nabla_{Decoder} L_2 \end{aligned}$$

end

features. In the second procedure, the memory bank in MAM is fixed, and the Encoder, Decoder, and FRM are optimized by training artificial negative samples, so that the FRM learns how to forget and input. As shown in Fig. 5 (a), in training stage 1, considering that the model optimized with L2-norm will produce blurry reconstructed images, L1-norm is used as the criterion for measuring distance:

$$L_{rec1} = \left| I_p - I_p' \right|_1 \tag{10}$$

Where  $|\cdot|_1$  denotes the L1-norm. To facilitate the sparsity of the generated addressing weights, as described in Section 3.4.1, CMA-AE is trained with the sparsity loss  $L_s$ . Therefore, the overall model is optimized under the joint loss function:

$$L_1 = w_1 L_{rec1} + w_2 L_s (11)$$

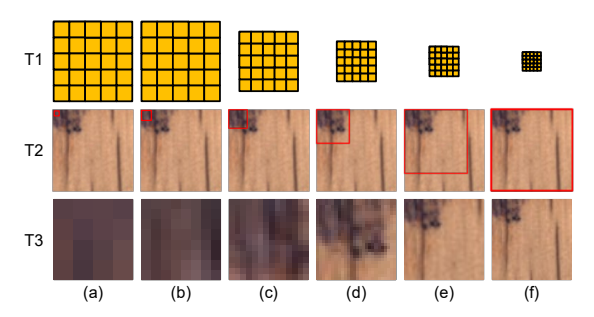


Fig 6. Different receptive fields of different scale. (a), (b), (c), (d), (e), and (f) are the receptive fields obtained by scale 1, scale 2, scale 3, scale 4, scale 5 and scale 6.

Where  $w_1$ ,  $w_2$  are the weights that control the relative importance of two terms. In this paper, we recommend setting  $w_1 = 50$  and  $w_2 = 0.01$ .

As shown in Fig. 5 (b), in training stage 2, same as training stage 1, L1-norm is used as the criterion for measuring distance:

$$L_{rec2} = |I_{an} - I'_{an}|_{1} \tag{12}$$

MAM is fixed, Encoder, FRM, and Decoder are optimized under the following joint loss function:

$$L_2 = W_1 L_{rec2} + W_2 L_s \tag{13}$$

The values of  $w_1$ ,  $w_2$  are the same as in the training stage 1. Finally, we summarize the two-stage training strategy in Algorithm 1.

## 3.5 Multi scale feature residual

In fact, anomalies are composite representations of multiple pixels with contextual relationships and have significant multi-scale properties. Therefore, to obtain accurate and noise-free anomaly segmented images, we propose MSFR. At first, we use the residual of feature maps instead of residual of images, which guarantees the correlation between pixels. An element in the feature map corresponds to a region in the original image, which can be thought of as an anomaly score for that region, as shown in Fig.6. However, as the receptive field expands as layer deepens,

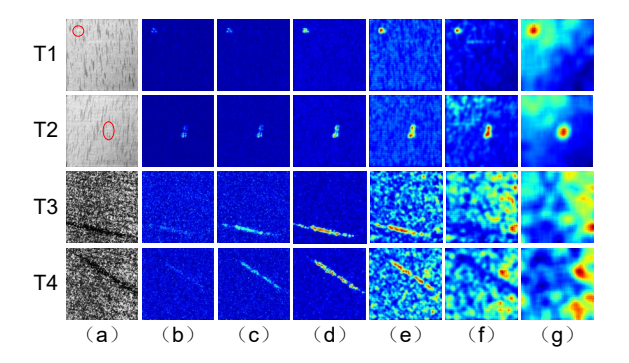


Fig 7. Feature residual by the proposed MSFR. (a) are defective images, (b), (c), (d), (e), (f), and (g) are the error maps obtained by scale 1, scale 2, scale 3, scale 4, scale 5 and scale 6.

an element in the feature map corresponds to a larger area of the image. When there are abnormal areas and normal areas exist at the same time, there will be errors wen the element is represented as normal or abnormal. To address this tradeoff, we use multiple feature residuals to obtain multi-scale information.

In many existing methods [6,25], VGG is trained as a feature extraction network on large-scale datasets, such as ImageNet [38]. These networks generalize well, but do not work for specific data. In this paper, the Encoder of CMA-AE can be regarded as a feature extractor learned from self-supervised learning on a specific dataset. Experiment 4 also proves the effectiveness of the Encoder. As shown in Fig. 2, in MSFR, when testing, the images and the corresponding reconstructions are fed to the Encoder, so we can get the multi-scale feature maps. However, not all feature maps can clearly express abnormal regions. We perform some experiments and analysis on the selection of feature maps. As illustrated in table I, the Encoder has a total of 6 convolutional layers. As depicted in Fig. 7, the error maps of scale 4, 5, 6 have a lot of noise. In this paper, we select the feature maps of scale 1, 2, 3 to obtain abnormal segmentation results.

Then, the feature maps are subtracted and squared, unsampled to the size of the original image, and averaged over the channel dimension. Finally, a weighted average of feature residuals at multiple scales is performed. The images is represented by  $I_n, I'_n \in R^{C \times H \times W}$ , the feature maps of

Table II Summarizes of the test datasets

Dataset	Tile	Cement Wallpaper		Carpet	Wood
Positive samples	509	492	267	280	247
Negative samples	150	150	300	89	60

scale 1, 2, 3 is represented by  $F_1, F_1' \in R^{C_1 \times H_1 \times W_1}$ ,  $F_2, F_2' \in R^{C_2 \times H_2 \times W_2}$ ,  $F_3, F_3' \in R^{C_3 \times H_3 \times W_3}$ , and the corresponding receptive field is represented by  $RF \in R^{C_1' \times H_1' \times W_1'}$ ,  $RF \in R^{C_2' \times H_2' \times W_2'}$ ,  $RF \in R^{C_3' \times H_3' \times W_3'}$ . Therefore,  $MSFR(I_n, I_n') \in R^{H \times W}$  are defined as follows:

$$MSFR(I_n, I'_n) = (\sum_{i=1}^{3} (H'_i \times W'_i) \times \delta(\tau((F_i - F'_i)^2))) / (\sum_{i=1}^{3} (H'_i \times W'))$$
(14)

where  $\delta(\cdot)$  is the operation that takes the mean in the channel dimension, and  $\tau(\cdot)$  is a a bilinear up-sampling function that resizes the feature tensors to  $H \times W$ .

## 4. Experimentation

# 4.1 Setup

In this section, we analyze the performance of the proposed CMA-AE method through several sets of experiments:

- a) The overall inspection performance of CMA-AE is qualitatively and quantitatively compared with eleven state-of-the-art methods on five benchmark datasets.
- b) The influences of each component in the CMA-AE have been explored in ablation experiments.
- c) The proposed MSFR are compared with the perceptual distance (PD) [43] in TrustMAE [25].

In these experiments, a variety of anomaly detection samples are used, including tile, cement, wallpaper, carpet and wood. The tile, cement and wallpaper datasets are sourced from DAGM [41],

Table III Experimental results of quantitative analysis

Dataset	Tile	Cement	Wallpaper	Carpet	Wood	
РНОТ	0.262	0.011	0.132	0.106	0.219	
TEXEMS	0.411	0.285	0.142	0.033	0.238	
AE	0.194	0.217	0.391	0.088	0.127	
AAE	0.174	0.190	0.333	0.089	0.264	
GPND	0.032	0.087	0.213	0.059	0.151	
OCGAN	0.242	0.167	0.085	0.284	0.373	
AE-SSIM	0.010	0.158	0.513	0.024	0.100	
MS-FCAE	0.340	0.079	0.112	0.184	0.222	
Ganomaly(patch)	0.596	0.003	0.554	0.453	0.520	
MemAE(patch)	0.593	0.001	0.768	0.335	0.505	
AFEAN	0.624	0.734	0.852	0.513	0.527	
Ours	0.841	0.792	0.902	0.571	0.703	

the carpet and wood datasets are sourced from MV-TAD [42]. Table II summarizes the datasets. All images are resized to 512x512 pixels.

To quantitatively analyze the performance of various methods, we use the quantitative metric F1-measure, which has been widely used in the performance evaluation of anomaly detection.

$$Recall = TP/(TP + FN) \times 100\%$$
 (15)

$$Precision = TP/(TP + FP) \times 100\%$$
 (16)

F1-Measure = 
$$(2 \times Precision \times Recall)/(Precision + Recall)$$
 (17)

where TP represents the number of correctly detected anomaly pixels in the anomaly foreground region, FP represents the number of falsely detected anomaly pixels in the normal background region, FN represents the number of undetected anomaly pixels in the anomaly region.

All the experiments are implemented using Python 3.8.0 and Pytorch 1.9.1 on a computer with two NVIDIA Tesla A100 GPU, which is equipped with 40 Intel(R) Xeon(R) CPU E5-2640 v4 at 2.40GHz and 40 GB memory.

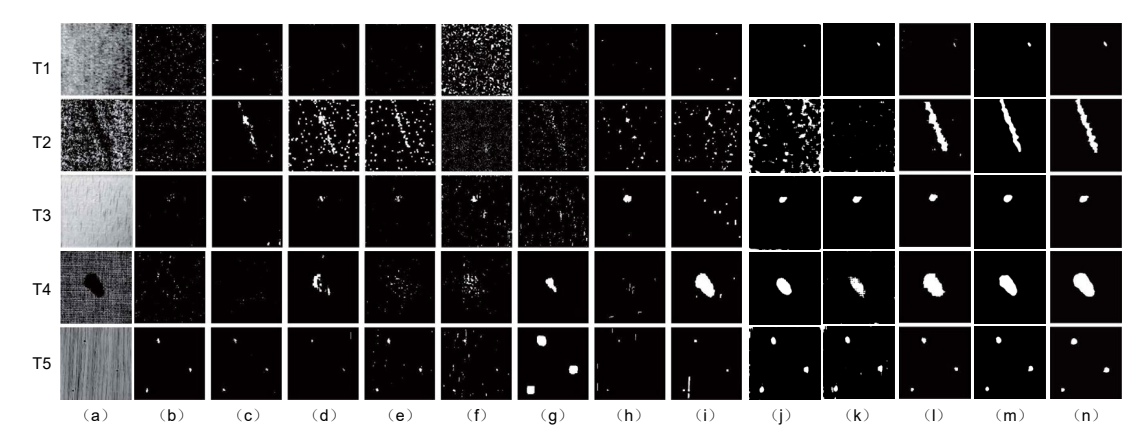


Fig 8. Examples of the defect inspection performances of the compared methods. T1, T2, T3, T4 and T5 are tile, cement, wallpaper, carpet and wood samples. (a) are the input images. (b)-(n) are PHOT[3], TEXEMS[4], AE[15], AAE[31], GPND[33], OCGAN[32], AE-SSIM[24], GANomaly[34], MemAE [16], AFEAN[18], Ours, and Ground Truth.

# 4.2 Overall Performance Comparison

To verify the overall performance of the proposed CMA-AE method, the inspection performance of CMA-AE is compared with a variety of excellent anomaly detection methods, including traditional methods (PHOT [3] and TEXTMS [4]) and unsupervised learning methods (AE [15], AAE [31], GPND [33], OCGAN [32], AE-SSIM [24], MS-FCAE [23], GANomaly [34], MemAE [16] and AFEAN[18]) on five datasets, as shown in table III and Fig. 8.

#### 4.2.1 Qualitative analysis

Some inspection results are shown in Fig. 8. The traditional methods (PHOT [3] and TEXTMS [4]) only perform well on the wood datasets and less well on other datasets, confirming our point that traditional methods are less robust. In contrast, methods including AE [15], AAE [31], GPND [33], OCGAN [32], AE-SSIM [24], MS-FCAE [23], GANomaly [34] and MemAE [16] can learn deeper feature representations for normal backgrounds from a large amount of data, with good generalization. However, the above methods cannot directly solve the anomality, resulting in miss inspection of cement sample. AFEAN [18] and CMA-AE perform well on cement sample. However, AFEAN adopts residual between original image and reconstructed image to segment defect, which

Table IV Experimental results of ablation study

Module	A	В	С	D	Е	F
Encoder	√	√	√	√	√	√
Decoder	√	√	√	√	√	√
CMAM(√)/MAM( * )/Cat( # )	√	*	#	<b>V</b>	<b>V</b>	
Two-stage training strategy	√	√	√	√		
MSFR	√	√	√		√	
F1-Measure	0.571	0.474	0.534	0.517	0.353	0.272

leads to a lot of noise. CMA-AE uses multi-scale feature residuals to segment defects, which makes defect segmentation more accurate and suppresses noise.

#### 4.2.2 Quantitative analysis

The experimental results of quantitative analysis are presented in Table III. CMA-AE outperforms other methods in F1-measure metric. Compared to the second-best results, CMA-AE improves F1-measure by margins of 0.217, 0.058, 0.050, 0.058 and 0.176 on the five-class samples. CMA-AE performs well on five different samples, which shows that our method has good generalization ability and can maintain performance on a variety of samples.

Extensive experiments show that CMA-AE achieves the best performance among all the compared methods in the test datasets. This performance improvement is due to the fact that our model can simultaneously repair anomalous foregrounds and reconstruct normal backgrounds, and employ MSFR methods to accurately segment defects.

## 4.3 Ablation study of CMA-AE

A set of ablation experiments are performed to confirm the influence of each module in CMA-AE. For a fair comparison, all evaluated variants of CMA-AE use the same parameter setting. The experimental results are shown in Table IV and Fig. 9.

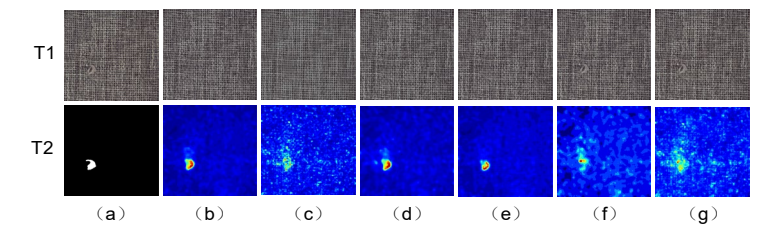


Fig 9. Examples of images from tests in the ablation study. T1 shows the reconstruct images, and the T2 shows the error maps. (a) is the defective image and Ground Truth. (b)-(f) are the result of the whole CMA-AE model, CMA-AE replacing CMAM with MAM, CMA-AE replacing forgetting and inputting gate with concatenate, CMA-AE without MSFR, CMA-AE without two-stage training strategy and the model only using Encoder and Decoder.

#### 4.3.1 Influence of CMAM

CMAM is proposed to solve the problem that MemAE [16] enhances the repair ability of abnormal foregrounds but weakens the ability to reconstruct normal backgrounds at the same time. In order to verify whether our improvement is effective, the impact of replacing CMAM with MAM will then be analyzed in detail next.

As shown in rows (b) and (c) of Fig. 9, after replacing CMAM with MAM, we find that its background is not reconstructed well, resulting in a lot of noise during defect segmentation. Table IV presents the experimental results, where CMA-AE (column A) improves the F1-measure by 0.088 compared to the model (column B) that replaced CMAM with MAM.

To verify that CMAM outperforms MAM not due to the increase of parameters, we design a set of comparative experiment between CMA-AE and Cat, replacing forget and input gates with concatenate. As shown in rows (b) and (d) of Fig. 9, we find that the error map of CMAM is clearer than that of Cat. Table IV presents the experimental results, where CMA-AE (column A) improves the F1-measure by 0.037 compared to the Cat (column C).

This experiment confirms that our CMAM outperforms MAM. CMAM can repair abnormal foreground through the way of forgetting and inputting, and can reconstruct normal background well, helping us achieve more accurate anomaly detection.

#### 4.3.2 Influence of MSFR

The purpose of MSFR is to accurately segment defects and reduce noise by exploiting feature residual at multiple scales. To verify the effectiveness, we removed the entire MSFR from CMA-AE.

Rows (b) and (d) of Fig. 9 show examples of the influence of MSFR. The model without MSFR result in inaccurate defect segmentation and a lot of noise. By using multi-scale feature residual, noise can be effectively suppressed and defect segmentation is more accurate. The experimental results are presented in table IV. CMA-AE [row(b)] improved the F1-measure by a magnitude of 0.087 compared to the model without MSFR [row(d)].

This experiment confirms that our MSFR is indeed effective. By exploiting multi-scale feature residuals, MSFR no longer focus on small gap between pixels, but on anomaly scores in regions of different sizes. This helps us achieve more accurate defect segmentation and suppress noise.

### 4.3.3 Influence of two-stage training strategy

The two-stage training strategy aims to let CMAM learn how to forget and input, giving the model the ability to distinguish abnormal foreground from normal background. To confirm its effectiveness, we removed the two-stage training strategy from CMA-AE.

Rows (b) and (e) of Fig 9 show an example of influence of two-stage training strategy. Without a two-stage training strategy, CMAM cannot learn how to forget and input, which results in good reconstruction of defects and undetectable defects in the testing phase. The experimental results are illustrated in Table IV, compared with model without the tow-stage training strategy [row(e)], CMA-AE [row (b)] improves F1-measure by 0.204.

The experiment confirms that our two-stage training strategy is effective. The two-stage

training strategy can make the model have the ability to distinguish abnormal foreground from normal background, which helps the model to better repair abnormal foreground.

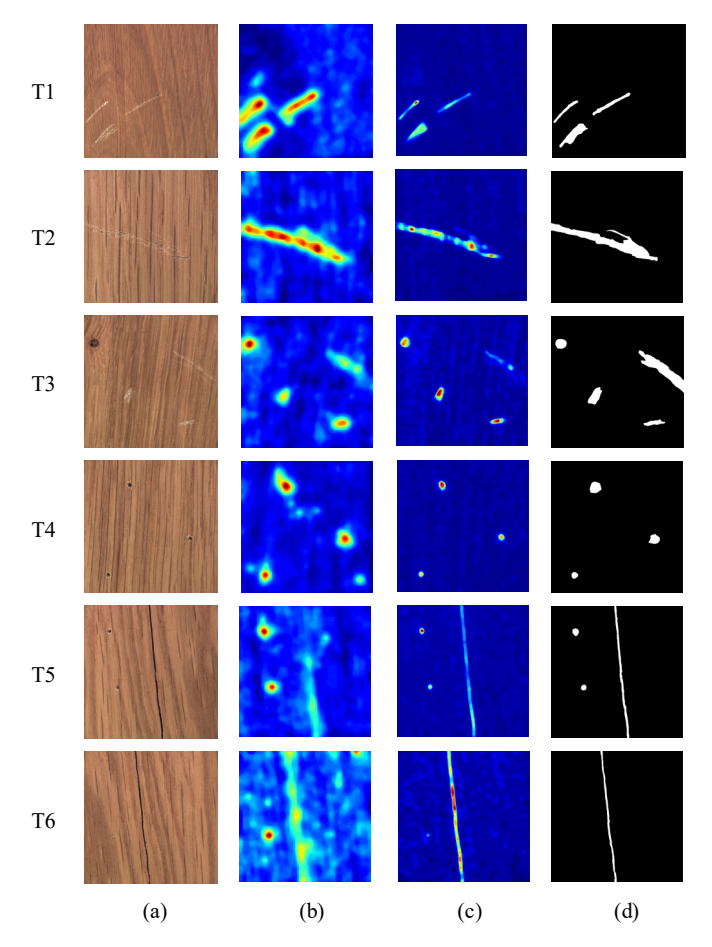


Fig 10. Examples of defect segmentation with PD and MSFR.(a) is the defective image,(b) is error map using PD,(c) is error map using MSFR,(d) is ground truth.

# 4.4 Comparative experiment of MSFR and PD

Similar to MSFR, TrustMAE [25] proposed to use PD [43] for defect segmentation, and its feature extractor is VGG-19 optimized using the Berkeley Adobe Perceptual Patch Similarity dataset. Although the neural network has good generalization, the feature extraction ability for different data is different. To verify that MSFR outperforms PD in TrustMAE, a set of comparative experiments was performed on the wood dataset.

Some results are shown in Fig. 10, the error maps of PD segmentation are very rough and have a lot of noise. This is because the pre-trained VGG-19 has poor feature extraction ability for surface

data and cannot distinguish abnormal foreground and normal background. The feature extractor selected by our method is the Encoder, which is trained on the surface dataset, so it has strong feature extraction ability for surface data and has good discriminative ability.

The experimental results of quantitative analysis are described in table VI. Compared with PD, MSFR improves F1-measure by 0.225.

## 5. Conclusion

In this paper, we proposed an unsupervised learning method CMA-AE for surface defect detection. This method is only trained on positive samples and artificial negative samples without any real negative samples. It is very important for the initial stage of the industrial production lines where negative samples are extremely scarce.

Academically, we divide the key points of reconstruction-based anomaly detection methods into anomaly foreground repair ability and normal background reconstruction ability. A novel CMAM module and a new method of two-stage training strategy are proposed to obtain the two abilities. Furthermore, MSFR is proposed for more accurate and reasonable defect segmentation. We observed that MSFR outperforms the traditional method based on pixel gaps between original image and reconstructed image. Because MSFR uses encoders as feature extractors, it is suitable for all the auto-encoder-based or GAN-based methods.

Extensive experimental results on several typical anomaly detection datasets show that our method CMA-AE achieves state-of-the-art detection accuracy. The performances may be further enhanced by improving GAAGA, such as edge of the weakening. In future research, we will focus on improving GAAGA to simulate more realistic defects.

## Acknowledgement

This work is supported by National Natural Science Foundation of China (51775214).

# References

- [1] K. Zhang, Y. Yan, P. Li, J. Jing, X. Liu, Z. Wang, Fabric defect detection using salience metric for color dissimilarity and positional aggregation, IEEE Access. 6 (2018) 49170–49181.
- [2] H. Wang, J. Zhang, Y. Tian, H. Chen, H. Sun, K. Liu, A simple guidance template-based defect detection method for strip steel surfaces, IEEE Transactions on Industrial Informatics. 15 (2018) 2798–2809.
- [3] D. Aiger, H. Talbot, The phase only transform for unsupervised surface defect detection, in: Emerging Topics In Computer Vision And Its Applications, World Scientific, 2012: pp. 215–232.
- [4] X. Xie, M. Mirmehdi, TEXEMS: Texture exemplars for defect detection on random textured surfaces, IEEE Transactions on Pattern Analysis and Machine Intelligence. 29 (2007) 1454– 1464.
- [5] W.-C. Li, D.-M. Tsai, Defect inspection in low-contrast LCD images using Hough transform-based nonstationary line detection, IEEE Transactions on Industrial Informatics. 7 (2009) 136–147.
- [6] H. Dong, K. Song, Y. He, J. Xu, Y. Yan, Q. Meng, PGA-Net: Pyramid feature fusion and global context attention network for automated surface defect detection, IEEE Transactions on Industrial Informatics. 16 (2019) 7448–7458.
- [7] D. Tabernik, S. Šela, J. Skvarč, D. Skočaj, Segmentation-based deep-learning approach for surface-defect detection, Journal of Intelligent Manufacturing. 31 (2020) 759–776.
- [8] V. Zavrtanik, M. Kristan, D. Skočaj, Reconstruction by inpainting for visual anomaly detection, Pattern Recognition. 112 (2021) 107706.
- [9] X. Zhang, J. Mu, X. Zhang, H. Liu, L. Zong, Y. Li, Deep anomaly detection with self-supervised learning and adversarial training, Pattern Recognition. 121 (2022) 108234.
- [10] M. Cho, T. Kim, W.J. Kim, S. Cho, S. Lee, Unsupervised video anomaly detection via normalizing flows with implicit latent features, Pattern Recognition. 129 (2022) 108703.
- [11] M. Ribeiro, A.E. Lazzaretti, H.S. Lopes, A study of deep convolutional auto-encoders for anomaly detection in videos, Pattern Recognition Letters. 105 (2018) 13–22.
- [12] Y. Zhou, B. Li, J. Wang, E. Rocco, Q. Meng, Discovering Unknowns: Context-enhanced Anomaly Detection for Curiosity-driven Autonomous Underwater Exploration, Pattern Recognition. (2022) 108860.
- [13] D. Chen, L. Yue, X. Chang, M. Xu, T. Jia, NM-GAN: Noise-modulated generative adversarial network for video anomaly detection, Pattern Recognition. 116 (2021) 107969.
- [14] J. Yang, Y. Shi, Z. Qi, Learning Deep Feature Correspondence for Unsupervised Anomaly Detection and Segmentation, Pattern Recognition. (2022) 108874.
- [15] G.E. Hinton, R.R. Salakhutdinov, Reducing the dimensionality of data with neural networks, Science. 313 (2006) 504–507.

- [16] D. Gong, L. Liu, V. Le, B. Saha, M.R. Mansour, S. Venkatesh, A. van den Hengel, Memorizing normality to detect anomaly: Memory-augmented deep autoencoder for unsupervised anomaly detection, in: Proceedings of the IEEE/CVF International Conference on Computer Vision, 2019: pp. 1705–1714.
- [17] A. Graves, Long short-term memory, Supervised Sequence Labelling with Recurrent Neural Networks. (2012) 37–45.
- [18] H. Yang, Q. Zhou, K. Song, Z. Yin, An anomaly feature-editing-based adversarial network for texture defect visual inspection, IEEE Transactions on Industrial Informatics. 17 (2020) 2220– 2230.
- [19] C. Lv, F. Shen, Z. Zhang, D. Xu, Y. He, A novel pixel-wise defect inspection method based on stable background reconstruction, IEEE Transactions on Instrumentation and Measurement. 70 (2020) 1–13.
- [20] C.-L. Li, K. Sohn, J. Yoon, T. Pfister, Cutpaste: Self-supervised learning for anomaly detection and localization, in: Proceedings of the IEEE/CVF Conference on Computer Vision and Pattern Recognition, 2021: pp. 9664–9674.
- [21] I. Goodfellow, J. Pouget-Abadie, M. Mirza, B. Xu, D. Warde-Farley, S. Ozair, A. Courville, Y. Bengio, Generative adversarial nets, Adv Neural Inf Process Syst. 27 (2014).
- [22] S. Mei, H. Yang, Z. Yin, An unsupervised-learning-based approach for automated defect inspection on textured surfaces, IEEE Transactions on Instrumentation and Measurement. 67 (2018) 1266–1277.
- [23] H. Yang, Y. Chen, K. Song, Z. Yin, Multiscale feature-clustering-based fully convolutional autoencoder for fast accurate visual inspection of texture surface defects, IEEE Transactions on Automation Science and Engineering. 16 (2019) 1450–1467.
- [24] P. Bergmann, S. Löwe, M. Fauser, D. Sattlegger, C. Steger, Improving unsupervised defect segmentation by applying structural similarity to autoencoders, ArXiv Preprint ArXiv:1807.02011. (2018).
- [25] D.S. Tan, Y.-C. Chen, T.P.-C. Chen, W.-C. Chen, TrustMAE: A noise-resilient defect classification framework using memory-augmented auto-encoders with trust regions, in: Proceedings of the IEEE/CVF Winter Conference on Applications of Computer Vision, 2021: pp. 276–285.
- [26] J. Hou, Y. Zhang, Q. Zhong, D. Xie, S. Pu, H. Zhou, Divide-and-assemble: Learning block-wise memory for unsupervised anomaly detection, in: Proceedings of the IEEE/CVF International Conference on Computer Vision, 2021: pp. 8791–8800.
- [27] T. Karras, S. Laine, T. Aila, A style-based generator architecture for generative adversarial networks, in: Proceedings of the IEEE/CVF Conference on Computer Vision and Pattern Recognition, 2019: pp. 4401–4410.
- [28] A. Frühstück, K.K. Singh, E. Shechtman, N.J. Mitra, P. Wonka, J. Lu, InsetGAN for Full-Body Image Generation, ArXiv Preprint ArXiv:2203.07293. (2022).
- [29] T. Schlegl, P. Seeböck, S.M. Waldstein, U. Schmidt-Erfurth, G. Langs, Unsupervised anomaly detection with generative adversarial networks to guide marker discovery, in: International Conference on Information Processing in Medical Imaging, Springer, 2017: pp. 146–157.
- [30] T. Schlegl, P. Seeböck, S.M. Waldstein, G. Langs, U. Schmidt-Erfurth, f-AnoGAN: Fast unsupervised anomaly detection with generative adversarial networks, Med Image Anal. 54 (2019) 30–44.

- [31] A. Makhzani, J. Shlens, N. Jaitly, I. Goodfellow, B. Frey, Adversarial autoencoders, ArXiv Preprint ArXiv:1511.05644. (2015).
- [32] P. Perera, R. Nallapati, B. Xiang, Ocgan: One-class novelty detection using gans with constrained latent representations, in: Proceedings of the IEEE/CVF Conference on Computer Vision and Pattern Recognition, 2019: pp. 2898–2906.
- [33] S. Pidhorskyi, R. Almohsen, G. Doretto, Generative probabilistic novelty detection with adversarial autoencoders, Adv Neural Inf Process Syst. 31 (2018).
- [34] S. Akcay, A. Atapour-Abarghouei, T.P. Breckon, Ganomaly: Semi-supervised anomaly detection via adversarial training, in: Asian Conference on Computer Vision, Springer, 2018: pp. 622–637.
- [35] S. Akçay, A. Atapour-Abarghouei, T.P. Breckon, Skip-ganomaly: Skip connected and adversarially trained encoder-decoder anomaly detection, in: 2019 International Joint Conference on Neural Networks (IJCNN), IEEE, 2019: pp. 1–8.
- [36] T. Niu, B. Li, W. Li, Y. Qiu, S. Niu, Positive-Sample-Based Surface Defect Detection Using Memory-Augmented Adversarial Autoencoders, IEEE/ASME Transactions on Mechatronics. (2021).
- [37] X. Shi, Z. Chen, H. Wang, D.-Y. Yeung, W.-K. Wong, W. Woo, Convolutional LSTM network: A machine learning approach for precipitation nowcasting, Adv Neural Inf Process Syst. 28 (2015).
- [38] J. Deng, W. Dong, R. Socher, L.-J. Li, K. Li, L. Fei-Fei, Imagenet: A large-scale hierarchical image database, in: 2009 IEEE Conference on Computer Vision and Pattern Recognition, Ieee, 2009: pp. 248–255.
- [39] J. Weston, S. Chopra, A. Bordes, Memory networks, ArXiv Preprint ArXiv:1410.3916. (2014).
- [40] J. Rae, J.J. Hunt, I. Danihelka, T. Harley, A.W. Senior, G. Wayne, A. Graves, T. Lillicrap, Scaling memory-augmented neural networks with sparse reads and writes, Advances in Neural Information Processing Systems. 29 (2016).
- [41] M. Wieler, T. Hahn, Weakly supervised learning for industrial optical inspection, in: DAGM Symposium In, 2007.
- [42] P. Bergmann, M. Fauser, D. Sattlegger, C. Steger, MVTec AD--A comprehensive real-world dataset for unsupervised anomaly detection, in: Proceedings of the IEEE/CVF Conference on Computer Vision and Pattern Recognition, 2019: pp. 9592–9600.
- [43] R. Zhang, P. Isola, A.A. Efros, E. Shechtman, O. Wang, The unreasonable effectiveness of deep features as a perceptual metric, in: Proceedings of the IEEE Conference on Computer Vision and Pattern Recognition, 2018: pp. 586–595.